DiVA
http://www.diva-portal.org

Postprint

This is the accepted version of a paper presented at *022 RIVF International Conference on Computing and Communication Technologies, RIVF 2022, Ho Chi Minh City, 20 December through 22 December 2022*.

Citation for the original published paper:

Vu, V T., Pernstal, T., Sjogren, T K., Pettersson, M. (2022)
Image extra-coregistration based on GIP for radar applications
In: Bao V.N.Q., Ha T.M. (ed.), *Proceedings - 2022 RIVF International Conference on Computing and Communication Technologies, RIVF 2022* (pp. 274-278). Institute of Electrical and Electronics Engineers (IEEE)
https://doi.org/10.1109/RIVF55975.2022.10013837

N.B. When citing this work, cite the original published paper.

©2022 IEEE. Personal use of this material is permitted. Permission from IEEE must be obtained for all other uses, in any current or future media, including reprinting/republishing this material for advertising or promotional purposes, creating new collective works, for resale or redistribution to servers or lists, or reuse of any copyrighted component of this work in other works.

Permanent link to this version:
http://urn.kb.se/resolve?urn=urn:nbn:se:bth-24291

Image extra-coregistration based on GIP for radar applications

1st Viet T. Vu
Blekinge Institute of Technology
Karlskrona, Sweden
viet.thuy.vu@bth.se

2nd Thomas Pernstål
SafeRadar
Mölndal, Sweden
thomas.pernstal@saferadar.se

3rd Thomas K. Sjögren
Swedish Defense Research Agency
Linköping, Sweden
thomas.sjogren@foi.se

4th Mats I. Pettersson
Blekinge Institute of Technology
Karlskrona, Sweden
mats.pettersson@bth.se

***Abstract*—Image coregistration is a mandatory procedure for radar applications such as synthetic aperture radar change detection. The spatial coregistration can be easily handled with geo-reference, whereas radiometric coregistration requires much more effort due to the randomness of noise and clutter. The performance of a coregistration method is usually measured by the correlation coefficient that is desire to be close to unity. However, the currently used methods cannot provide coregistration with such correlation coefficient value. The paper introduces an image extra-coregistration method that helps to increase the correlation coefficient between the radar images close to unity. This strongly supports radar applications such as change detection.**

***Index Terms*—Coregistration, radar, image, VHF**

I. Introduction

Image coregistration refers to methods that are used to align two or more radar images of a ground scene in order to make them correlate. Image coregistration is mandatory for several radar applications such as synthetic aperture radar change detection. Assume that the same radar system has been used to illuminate a ground scene several times (passes) and the multipass data is used to form the radar images. If the time separation between the illuminations is short, the differences between the images come mainly from clutter and noise. For example, small differences in flight paths during the multiple passes can lead to different reflections of the clutter and therefore the differences between images. For radar applications like change detection, these differences can lead to detection failure and/or false alarms. A good coregistration method is therefore seen as prerequisite for such applications.

Several coregistration methods have been emerged recently. In [1], the coregistration of multipass radar images based on isolated point-like scatterers analysis is introduced. In [2], a SAR image co-registration procedure, based on the use of external measures is discussed. In [3], a new strategy that uses a sample offset series of detected subimage patches dominated by point-like scatterers to improve image coregistration is proposed. For practical radar systems, special coregistration procedures are designed for them. We take a CARABAS image set as an example [4]. The image set is formed with the data measured in several passes by the same radar system following the same flight path. The images are geo-referenced to the same ground coordinate system and radio-metrically calibrated. Spectral filtering and geographical registration can also be applied to the images to increase the correlation between images. The frequency band is in the range 25-85 MHz and the aperture integration angle is 70°. However, the correlation coefficient, that is usually used to evaluate the performance of coregistration and desired to be unity, is still under the expectation although the time separation between measurements is short, e.g., less than 1 hour. This can be explained by the dominant of clutter and noise in the radar images that are not easy to be equalized. Hence, extra-coregistration is therefore necessary in this case. A similar set is utilized for the experiments in this study. The image set is formed with the data recently measured in 4 passes by LORA operating in the VHF band.

The method for interference detection and mitigation based on generalized inner product (GIP) was introduced recently in [5]. The method was developed to detect interference that can modify radar signals. To detect the interference, GIP is computed for the radar signals. If GIP is under a pre-defined threshold, no interference will be declared. In the opposite case, the interference will be detected and mitigated with an interference removal procedure. The method has been tested successfully with different radar measurements.

In this paper, we introduce an image extra-coregistration for radar applications. The clutter and noise detection are based on GIP computed on the multipass radar images and the same interference removal procedure proposed in [5] is used for equalizing the clutter and noise in the multipass radar images. It should be highlighted that in a radar image, clutter and noise are dominant that is opposite to the case presented in [5], where the radar signal is dominant.

The rest of the paper is organized as follows. Sections II presents the method for interference detection and mitigation based on GIP. The extra-coregistration method is presented in Section III. The experimental results on the image set that has

been coregistered are provided in Section IV. Section V gives the conclusions.

II. Interference detection and mitigation based on GIP

The method for interference detection and mitigation based on GIP is introduced in [5]. As known, GIP can be used to measure the homogeneity of the data contents. For a complex Gaussian distributed vector $\mathbf{z} = [z_1, z_2, \cdots, z_M]$ with zero mean and known positive definite Hermitian covariance matrix $\mathbf{R}$, i.e., $\mathbf{z} \sim CN(0, \mathbf{R})$, the quadratic form $\mathbf{z}^{\mathrm{H}}\mathbf{R}^{-1}\mathbf{z}$ has mean N and is chi-square distributed with M complex degrees of freedom. The Hermitian covariance matrix is generally unknown, requiring $\mathbf{R}$ be replaced by the sample covariance matrix, $\hat{\mathbf{R}}$, commonly retrieved from the maximum-likelihood estimate.

Let $\mathbf{Z}$ denote a data matrix, whose columns $\mathbf{z}_k$, $k = 1, 2, \cdots, K$ are independent and identically distributed $CN(\mathbf{0}, \mathbf{R})$, then the maximum-likelihood estimate for the Hermitian covariance matrix is

$$\hat{\mathbf{R}} = \frac{1}{K}\mathbf{Z}\mathbf{Z}^{\mathrm{H}} \tag{1}$$

A GIP statistical test is defined by

$$P_k = \mathbf{z}_k^{\mathrm{H}}\hat{\mathbf{R}}^{-1}\mathbf{z}_k \tag{2}$$

To detect interference existing in the data, a threshold λ is set on P_k. If we denote the outlier samples and the rest of sample set $\mathbf{Z_{out}}$ and $\mathbf{Z_{in}}$, respectively, then the data samples with and without interference are sorted out by

$$\mathbf{Z} = \begin{cases} \mathbf{Z_{out}} & \mathbf{z}_k^{\mathrm{H}}\hat{\mathbf{R}}^{-1}\mathbf{z}_k \geq \lambda \\ \mathbf{Z_{in}} & \mathbf{z}_k^{\mathrm{H}}\hat{\mathbf{R}}^{-1}\mathbf{z}_k < \lambda \end{cases} \tag{3}$$

The processing scheme to suppress the detected interference is shown in Fig. 1. According to the processing scheme, the data samples without interference $\mathbf{Z_{in}}$ are maintained without any modification. The interference existing in $\mathbf{Z_{out}}$ will be removed before combining with $\mathbf{Z_{in}}$ to form the new data.

To compute the interference covariance, it is required to pre-whiten the outlier samples by

$$\mathbf{Y_{out}} = \mathbf{Z_{out}}\hat{\mathbf{C}}^{-1} \tag{4}$$

where $\hat{\mathbf{C}}$ is a lower triangular matrix with real and positive diagonal entries obtained by the Cholesky decomposition of $\hat{\mathbf{R}}$. With the pre-whitening outlier samples, the covariance matrix, $\hat{\mathbf{R}}_{\mathbf{out}}$, originating from the interference is retrieved with the maximum-likelihood estimate

$$\hat{\mathbf{R}}_{\mathbf{out}} = \frac{1}{L}\mathbf{Y_{out}}\mathbf{Y_{out}}^{\mathrm{H}} \tag{5}$$

where L is the number of columns of the matrix $\mathbf{Y_{out}}$ and $L < K$.

The interference existing in $\mathbf{Z_{out}}$ is mitigated by pre-whitening $\mathbf{Z_{out}}$ using the Cholesky decomposed version of $\hat{\mathbf{R}}_{\mathbf{out}}$

$$\tilde{\mathbf{Z}}_{\mathbf{out}} = \mathbf{Z_{out}}\hat{\mathbf{C}}_{\mathbf{out}}^{-1} \tag{6}$$

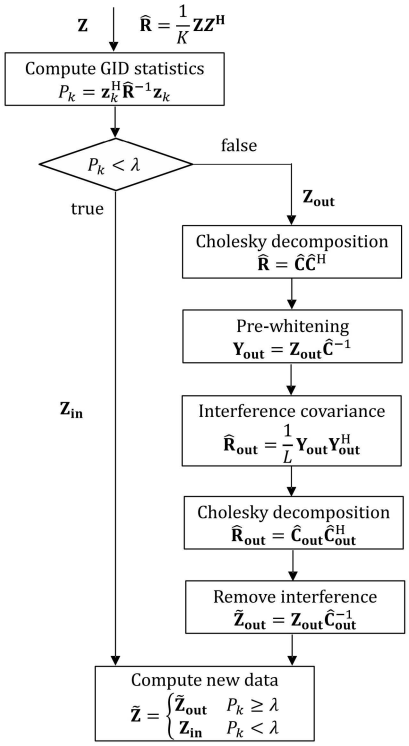

Fig. 1. Processing scheme for interference detection and suppression based on GIP.

where

$$\hat{\mathbf{R}}_{\mathbf{out}} = \hat{\mathbf{C}}_{\mathbf{out}}\hat{\mathbf{C}}_{\mathbf{out}}^{\mathrm{H}} \tag{7}$$

The new data with mitigated interference is computed with

$$\tilde{\mathbf{Z}} = \begin{cases} \tilde{\mathbf{Z}}_{\mathbf{out}} & \mathbf{z}_k^{\mathrm{H}}\hat{\mathbf{R}}^{-1}\mathbf{z}_k \geq \lambda \\ \mathbf{Z_{in}} & \mathbf{z}_k^{\mathrm{H}}\hat{\mathbf{R}}^{-1}\mathbf{z}_k < \lambda \end{cases} \tag{8}$$

III. Extra-coregistration method

Assume that two synthetic aperture radar measurements carried out with the identical flight paths, called passes, and aim at the same geographical area. The separation in time between two measurements is small, e.g., less than 1 hour, so that the changes in the SAR scene are insignificant. The measured complex data is then used to form radar images, called reference and surveillance. In theory, the reference and surveillance images are almost identical. The small differences between two images may come from the small changes in the ground scene between two measurements separated in time. In practice, the reference and surveillance images are geo-referenced to the same ground coordinate system and a radiometric calibration is carried out. An addition coregistration procedure is also applied to the reference and surveillance images consisting of two processing steps:

- Spectral filtering
- Geographical registration

The spectral filtering step ensures the images within the same frequency range and limited by the same aperture integration

angle. In other words, the images should have the same region of support. It is also helps to reduce the frequency content to make analysis of different bandwidths within the full region of support possible. The geographical registration is seen as an extra spatial coregistration. Although the geo-referencing step is generally very accurate in aligning the reference and surveillance images, the geographical coregistration will ensure that the two images coincide. Through the geographical registration step, the reference and surveillance images are transformed from platform coordinates to map coordinates. An accurate geographical registration simplifies the problem of aligning the images. The images are projected into ground coordinates using GPS/IMU flight path data recorded onboard and a digital elevation model (DEM) of the ground topography. Among the processing step, geo-reference is shown to be the most important step that establishes the correlation between images. Other processing steps help to improve slightly the correlation. For this reason, the image set utilized for the experiments in this study is only geo-referenced.

The overall correlation between the reference and surveillance images is usually evaluated by the correlation coefficient that is defined by

$$\rho = \left| \frac{\sum \Im_r \bar{\Im}_s}{\sqrt{\sum \Im_r \bar{\Im}_r} \sqrt{\sum \Im_s \bar{\Im}_s}} \right| \tag{9}$$

where $\Im_r$ and $\Im_s$ denote the reference and surveillance image samples, respectively, the $\bar{\Im}$ denotes the conjugate complex operator.

The correlation coefficient is desired to approach unity since the changes in the ground scene in short time are insignificant. However, the noise, clutter and other interference spread over the images reduce the overall correlation between the reference and surveillance images significantly. The correlation coefficients obtained after radiometric calibration, geo-reference, spectral filtering, and geographical registration is usually below the expectation. This can be explained by the clutter and noise dominant in the radar images that are not easy to equalize.

In the following, an extra-coregistration method is introduced. The processing scheme of the method is like the one given in Fig. 1. However, the outlier samples must be maintained since they contain the information of interest, whereas the rest of sample set is expected to be equalized.

A. Extra coregistration

Let the complex vectors $\mathbf{s}$, $\mathbf{c}$, and $\mathbf{n}$ denote changes in ground scene or simply called target, clutter, and noise in a radar image.

$$\mathbf{s} = \begin{pmatrix} s_r \\ s_u \end{pmatrix} \qquad \mathbf{c} = \begin{pmatrix} c_r \\ c_u \end{pmatrix} \qquad \mathbf{n} = \begin{pmatrix} n_r \\ n_u \end{pmatrix} \tag{10}$$

where the subscript $_s$ and $_u$ refer to reference and surveillance (updated), respectively. The $k-$th data vector is defined by

$$\mathbf{z}_k = \mathbf{s}_k + \mathbf{c}_k + \mathbf{n}_k \tag{11}$$

Since clutter and noise are dominant in a radar image, the maximum-likelihood estimate for the Hermitian covariance matrix

$$\hat{\mathbf{R}} = \frac{1}{K}\mathbf{Z}\mathbf{Z}^{\mathrm{H}} = \frac{1}{K}\sum \mathbf{z}_k \mathbf{z}_k^{\mathrm{H}} \tag{12}$$

is a quite good estimate of the clutter and noise covariance matrix. The Hermitian covariance matrix $\hat{\mathbf{R}}$ will be a 2×2 matrix. Armed with $\hat{\mathbf{R}}$, we can calculate GIP for each data vector $\mathbf{z}_k$ and get P_k using (2). Assume that λ is a predefined threshold, (3) helps to sort out the outlier samples that may contain signal, clutter and noise ($\mathbf{Z_{out}}$), and the data samples that may contain only clutter and noise ($\mathbf{Z_{in}}$).

Because the outlier samples must be maintained since they contain the information of interest, i.e., change or signal, the selection structure of the processing scheme given in Fig. 1 is modified from $P_k < \lambda$ to $P_k > \lambda$. The new computed data is defined by

$$\tilde{\mathbf{Z}} = \begin{cases} \mathbf{Z_{out}} & \mathbf{z}_k^{\mathrm{H}} \hat{\mathbf{R}}^{-1} \mathbf{z}_k \geq \lambda \\ \tilde{\mathbf{Z}}_{\mathbf{in}} & \mathbf{z}_k^{\mathrm{H}} \hat{\mathbf{R}}^{-1} \mathbf{z}_k < \lambda \end{cases} \tag{13}$$

where $\tilde{Z}_{in}$ is computed with $\mathbf{Z_{in}}$ and $\hat{\mathbf{R}}$ by the interference mitigation procedure, i.e.,

$$\begin{cases} \hat{\mathbf{R}} = \hat{\mathbf{C}}\hat{\mathbf{C}}^{\mathrm{H}} \\ \mathbf{Y_{in}} = \mathbf{Z_{in}}\hat{\mathbf{C}}^{-1} \\ \hat{\mathbf{R}}_{\mathbf{in}} = \dfrac{1}{L}\mathbf{Y_{in}}\mathbf{Y_{in}}^{\mathrm{H}} \\ \hat{\mathbf{R}}_{\mathbf{in}} = \hat{\mathbf{C}}_{\mathbf{in}}\hat{\mathbf{C}}_{\mathbf{in}}^{\mathrm{H}} \\ \tilde{\mathbf{Z}}_{\mathbf{in}} = \mathbf{Z_{in}}\hat{\mathbf{C}}_{\mathbf{in}}^{-1} \end{cases} \tag{14}$$

where L is the length of data that needs to be computed. The covariance matrix $\hat{\mathbf{R}}_{\mathbf{in}}$ is the covariance matrix of clutter and noise. The last computation in (14) gives therefore the equalized clutter and noise in the images.

B. Thresholding

Selecting threshold λ is critical. A wrong selection can degrade the overall correlation between the radar images. Several approaches for setting λ can be considered as follows.

A simple approach to set the threshold λ is based on the initial guess about the percentage of data with target (change). Because the clutter and noise are dominant in radar images, the percentage of data with target should be very small, e.g., $\epsilon = 5\%$. After calculating P_k, we can sort the values of P_k in a descending order. By this, the threshold λ can be easily retrieved based on ϵ. It is obvious this approach is simple and efficient in time. However, the approach may give low correlation coefficients in the case the threshold is higher than the value (percentage) in practice. Not all clutter and noise are considered for equalization. The approach may also result into high correlation coefficients in the case the threshold is lower than the value in practice. However, the signal can be eliminated in this case.

Another approach can be based on the fact that the expectation on the correlation coefficient can always be set. Threshold can then be regulated in an iterative way according to the desired correlation coefficient. In the first iteration, the

TABLE I
PARAMETERS OF LORA IN VHF BAND FOR MEASUREMENT CAMPAIGN.

System parameter	Configured value
Platform speed	128 m/s
Platform altitude	3500 m
Incidence angle	36°
Frequency range	19.2−90.9 MHz
Pulse repetition frequency	178 Hz
Aperture step	0.72 m
Coherent integration angle	108°
Minimum range	8915 m

percentage can be set higher than the value in practice, e.g., $\epsilon = 10\%$. A low correlation coefficient can be predicted. After each iteration, the percentage is reduced with a small step, e.g., $\Delta\epsilon = 1\%$. The iteration that the expected correlation coefficient is reached, will be the last iteration. It is obvious that setting threshold using this approach requires more computational burden.

In the following experiments, only the simple approach to set threshold is considered.

IV. EXPERIMENTAL RESULTS

The extra-coregistration method proposed in Section III is evaluated in this section based on the radar image set that relate to the measurement campaign in Karlskrona, Sweden in 2020 and 2021. The correlation coefficient given by (9) is used to regulate the threshold for an extra-coregistration but can also be seen as the assessment of the proposed extra-coregistration method.

A. Data description

The measurement campaign performed by LORA operating in the VHF band, a Swedish synthetic aperture radar system. The measurement campaign has different goals, in which providing data for the research about coregistration is one of them. Therefore, several radar measurements with identical flight paths have been carried out with different separations in time. For a short separation in time, two measurements were less than half an hour apart. For a long separation in time, the time distance was more than a year. The one of the outcomes of the measurement campaign is a image set with four images: two measured on 27 August 2020 separated by about half hour (image 1, image 2) and two measured on 6 October 2021 separated by about half hour (image 3, image 4). All images have been geo-referenced. Figure 2 shows the radar image 1, reconstructed from the data collected on 27 August 2020.

An image covers an area of $4.096 \times 4.096\,\mathrm{km}^2$. For the image pixel of 1×1 m^2, the matrix dimension of the SAR image is 4096×4.096 elements. The column and the row of the matrix correspond to the azimuth direction and the range direction, respectively.

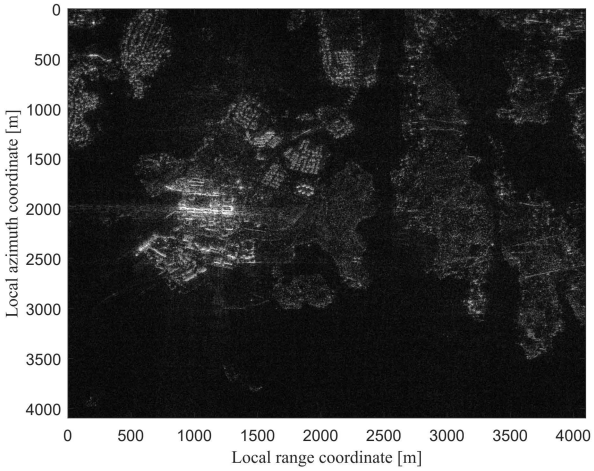

Fig. 2. Image of ground scene (Image 1).

The first part of Table II summarizes the computed correlation coefficients using (9) for all images. As observed, the correlation coefficients are below 0.85, even for the images corresponding to two measurements on the same day. For the images corresponding to two measurements with a long separation in time, the correlation coefficients drop below 0.6. An extra-coregistration for the images is necessary.

B. Extra-coregistration

With the set of 4 images, we can test the proposed extra-coregistration method on 6 pairs of reference and surveillance images:

$$\begin{pmatrix} \text{Image 1} \\ \text{Image 2} \end{pmatrix} \quad \begin{pmatrix} \text{Image 2} \\ \text{Image 3} \end{pmatrix} \quad \begin{pmatrix} \text{Image 3} \\ \text{Image 4} \end{pmatrix}$$

$$\begin{pmatrix} \text{Image 1} \\ \text{Image 2} \end{pmatrix} \quad \begin{pmatrix} \text{Image 2} \\ \text{Image 4} \end{pmatrix} \quad \begin{pmatrix} \text{Image 3} \\ \text{Image 1} \end{pmatrix}$$

It is worth to highlight that the correlation coefficients reported in Table II cannot provide any information for setting the threshold λ. For the measurements with the short time separation, the number of changes in the ground scene is small. The ratio of the change area to the total area might be set less than $\epsilon < 1\%$. For the measurements with the long-time separation, the amount of changes in the ground scene can be larger. The ratio of the change area to the total area might be set by $\epsilon > 10\%$. Based on these percentages, we can easily find the thresholds applied for the images. In this experiment, we use $\epsilon = 0.5\%$ for the short-time separation case and $\epsilon = 10\%$ for the long-time separation case.

The performance of the extra-coregistration method is evaluated by the correlation coefficients and provided in the second part of Table II showing that the correlation between images is improved. For the images corresponding to the measurements with the short time separation, the correlation coefficients increase significantly up to 0.97. For the images corresponding

TABLE II
OVERALL CORRELATION BETWEEN IMAGES.

ρ	**Image 1**	**Image 2**	**Image 3**	**Image 4**
Coregistered images				
Image 1	1	0.844	0.5615	0.5424
Image 2	0.844	1	0.5632	0.5478
Image 3	0.5615	0.5632	1	0.7037
Image 4	0.5424	0.5478	0.7037	1
Extra-coregistered images				
Image 1	1	0.9081	0.9739	0.9689
Image 2	0.9081	1	0.9732	0.9688
Image 3	0.9739	0.9732	1	0.9046
Image 4	0.9689	0.9688	0.9046	1
Extra-coregistered image stack				
Image 1	1	0.9934	0.9837	0.9874
Image 2	0.9934	1	0.9848	0.9807
Image 3	0.9837	0.9848	1	0.9703
Image 4	0.9874	0.9807	0.9703	1

to the measurements with the long-time separation, the correlation coefficients can even increase up to 0.97. This indicates the influence of the threshold λ on the performance of the proposed method.

C. Extra coregistration for image stack

The proposed extra coregistration approach does not limit by a single reference image and a single surveillance image. It can be applied to image stacks with more than two images playing the roles of reference and/or surveillance. An extra-coregistration for image stack is also expected to give the same correlation coefficients for all images in the stack. With the given four images, we can form image stacks and perform extra-coegistration for the stacks

$$\begin{pmatrix} \text{Image 1} \\ \text{Image 2} \\ \text{Image 3} \\ \text{Image 4} \end{pmatrix}$$

This data matrix is now placed at the input of the proposed extra-coregistration method. It should be highlight that the Hermitian covariance matrix $\hat{\mathbf{R}}$ will be a 4×4 matrix. We use the same threshold with $\epsilon = 2\%$. The correlation coefficients computed with the new images are summarized in the third part of Table II showing that the overall correlation between the images is extremely improved and the correlation coefficients computed are all above 0.97.

V. CONCLUSIONS

In this paper, an image extra-coregistration method has been introduced that helps to increase the correlation coefficient between the radar images. This strongly supports radar applications such as change detection. The method has been tested with the radar images. The results show that the correlation between the images are improved significantly. The results also show the influence of the threshold on the performance of the image extra-coregistration method. The method has also been tested with the image stack. The result also shows an extreme improvement in the correlation between images in the stack.

REFERENCES

[1] F. Serafino, "SAR image coregistration based on isolated point scatterers," IEEE Geosci. Remote Sens. Lett., vol. 3, no. 3, pp. 354–358, 2006.

[2] E. Sansosti, P. Berardino, M. Manunta, F. Serafino, and G. Fornaro, "Geometrical SAR image registration," IEEE Trans. Geosci. Remote Sens., vol. 44, no. 10, pp. 2861–2870, 2006.

[3] T. Wang, S. Jonsson, and R.F. Hanssen, "Improved SAR image coregistration using pixel-offset series," IEEE Geosci. Remote Sens. Lett., vol. 11, no. 9, pp. 1465–1469, 2013.

[4] L.M.H. Ulander, M. Lundberg, W. Pierson, and A. Gustavsson, "Change detection for low-frequency SAR ground surveillance," IEE Proc. Radar Sonar Navig., vol. 152, no. 6, pp. 413–420, 2005.

[5] T. Pernstål, J. Degerman, H. Broström, V.T. Vu, and M.I. Pettersson, "GIP test for automotive FMCW interference detection and suppression," IEEE Radarconf20, Florence, Italy, pp. 1–6, Sept. 2020.